Incommensurate magnetic cycloidal order in noncentrosymmetric Eu_2Pd_2Sn

A. Martinelli,[1] D. H. Ryan,[2] J. G. Sereni,[3] C. Ritter,[4] I. Čurlík,[5] and M. Giovannini[6]
[1]*CNR-SPIN, Corso F. M. Perrone 24, 16152 Genova, Italy*
[2]*Physics Department and the Centre for the Physics of Materials, McGill University, 3600 University Street, Montreal, Quebec, Canada H3A 2T8*
[3]*Department of Physics, CAB-CNEA, CONICET, 8400 San Carlos de Bariloche, Argentina*
[4]*Institut Laue-Langevin, 71 Avenue des Martyrs, 38042 Grenoble Cedex 9, France*
[5]*Faculty of Humanities and Natural Sciences, University of Prešov, 17.novembra 1, Prešov, Slovakia*
[6]*Department of Chemistry and Industrial Chemistry, University of Genova, Via Dodecaneso 31, 16146 Genova, Italy*

(Received 8 January 2024; accepted 6 March 2024; published 21 March 2024)

The structural and magnetic properties of the noncentrosymmetric Eu_2Pd_2Sn compound have been investigated by synchrotron x-ray and neutron powder diffraction and ^{151}Eu Mössbauer spectroscopy. No structural transition was observed in the temperature range 4–290 K. The magnetic phase that develops below ∼13.8(5) K is characterized by an incommensurate cycloidal ordering in the ac plane of the Eu substructure. This magnetic structure shows significant analogies to the structure observed in $EuNiGe_3$, possibly indicating the occurrence of a skyrmion lattice for Eu_2Pd_2Sn as well.

DOI: 10.1103/PhysRevB.109.104424

I. INTRODUCTION

Magnetism in noncentrosymmetric (NCS) magnetic materials is of great interest due to topologically nontrivial magnetic textures, which offer the potential for new magnetic information manipulation and storage technologies [1,2]. This variety of complex magnetic order is due to the competition between the Heisenberg interaction, which favors ferromagnetic (FM) and antiferromagnetic states, and the Dzyaloshinskii-Moriya interaction (DMI), which causes clockwise or counterclockwise rotation of spins [3]. The presence of DMI requires the violation of inversion symmetry and the presence of a sizable spin-orbit coupling (SOC). In many cases, the spin structures are not collinear and are accompanied by incommensurate spiral arrangements, as in the case of the skyrmion lattice in MnSi [4] or in structurally related compounds such as EuPtSi [5]. While skyrmions usually occur in noncentrosymmetric materials (in bulk or induced by interfaces between materials), it was recently discovered that magnetic frustration in Gd compounds can also stabilize the skyrmion lattice [6]. In the absence of crystal field splitting, the total spin state $S = 7/2$ of Eu^{2+} and Gd^{3+} provides an ideal platform to study the formation of spin structures.

Most of the initial research on noncentrosymmetric complex spin structures was devoted to chiral lattice structures such as MnSi and isotypic compounds. In addition to the discovery of many intriguing properties, it was shown that structural chirality uniquely determines the magnetic chirality of these compounds [7]. More recently, attention has been focused on acentric crystals possessing vertical mirror planes including a proper axis (i.e., with *polar* point group), such as $EuTGe_3$ (T = transition metal) with the tetragonal $BaNiSn_3$−type structure (point group C_{4v}). The best studied of these compounds is $EuNiGe_3$, where helimagnetic order and the appearance of an anomalous Hall effect in the intermediate phase in a magnetic field could indicate the formation of a skyrmion lattice state [8]. In a recent work [9], we have shown that Eu_2Pd_2Sn, crystallizing in the noncentrosymmetric orthorhombic structure type (polar point group C_{2v}), exhibits significant similarities with $EuNiGe_3$; in particular, the magnetic transition occurs at about the same temperature ($T_m = 13$ K) and is followed by a broad hump in the specific heat (C_p) at about 10 K with a similar jump in magnetoresistance. Both the C_p and magnetoresistance anomalies in Eu_2Pd_2Sn were associated with a change in the incommensurate character of the magnetic structure at zero field ($B = 0$). At higher fields, the possibility of a skyrmionic pocket was suggested in the magnetic phase diagram of Eu_2Pd_2Sn, between a critical point CP_1 (∼7 K, 1.5 T) and 2 K, within the range $1.25 < B < 1.7$ T. The frustrated character of the puckered *ac* plane, the ∼65° dihedral angle between the Eu chains, and a possible modulated propagation vector support this possibility [9].

Neutron diffraction is by far the best method for determining a magnetic structure, but for Eu-based compounds this technique is hampered by the large thermal neutron absorption cross section characterizing natural europium. Nevertheless, neutron diffraction analysis for magnetic structure determinations can be carried out using a large-area flat-plate geometry [10], minimizing the effect of strong neutron absorption. In this way, our group determined the magnetic structure of several compounds belonging to the Eu-Pd-Sn ternary phase diagram. In EuPdSn the magnetic ordering at 16.2 K is followed by a change in the magnetic structure at ∼12 K; in particular, an incommensurate sinusoidally modulated magnetic structure is observed at 13.2 K, and this transforms into a planar helimagnetic structure at 3.6 K [11]. In $EuPdSn_2$, magnetic and antiferromagnetic domains coexist below 12 K and compete in the ground state [12].

In this work, we report the results of neutron diffraction and Mössbauer measurements on Eu_2Pd_2Sn, which show that its magnetic structure has analogies to that observed in $EuNiGe_3$, suggesting a possible skyrmion lattice also for Eu_2Pd_2Sn.

II. EXPERIMENT

A. Sample preparation and analyzes

Samples were prepared as described in Ref. [13]. Stoichiometric amounts of pure elements (Eu 99.99 mass % and Sn 99.999 mass % by Smart Elements, Vienna, Austria; Pd 99.5 mass % from Chimet, Arezzo, Italy) were weighed in a glove box and enclosed in tantalum crucibles sealed by arc welding under pure argon atmosphere. The reactant mixture was melted by using an induction furnace under a stream of pure argon and then annealed in a resistance furnace at 600° C for two weeks. Finally, the sample was quenched in cold water.

^{151}Eu Mössbauer spectroscopy measurements were carried out using a 3 GBq $^{151}SmF_3$ source, operated in sinusoidal mode. The drive motion was calibrated by a $^{57}CoRh/\alpha - Fe$ standard foil. Isomer shifts are quoted relative to EuF_3 at room temperature. The 21.6 keV gamma rays were recorded by a thin NaI scintillation detector. The sample was cooled in a vibration-isolated closed-cycle helium refrigerator with the sample in the helium exchange gas. The spectra were used to fit the parameters describing a sum of Lorentzian lines to the positions and intensities derived from a full solution of the nuclear Hamiltonian [14].

Synchrotron x-ray powder diffraction (XRPD) was carried out at the high-intensity–high-resolution ID22 beamline of the European Synchrotron Radiation Facility (ESRF), using a wavelength $\lambda = 0.3543$ Å. XRPD data were collected in the temperature range 5–290 K. A reference pattern from LaB_6 powder (NIST 660a) was acquired to evaluate the instrumental line broadening.

Neutron powder diffraction (NPD) was performed at the Institut Laue Langevin (ILL; Grenoble–F) using the high-intensity D20 diffractometer. NPD patterns were collected using a wavelength $\lambda = 2.414$ Å in the temperature range 2.5–20 K; in particular, higher statistic data were collected at 20 K (in the paramagnetic state) and at 10.7 and 2.5 K (below the magnetic transition temperature). To minimize the effect of the strong neutron absorption of natural Eu ($\sigma_{abs} = 4530$ b), a large-area sample holder with flat-plate geometry was used [10]; for this purpose, powdered Eu_2Pd_2Sn was dispersed and fixed in the single-crystal silicon flat-wafer sample holder with an alcoholic solution (ethanol) of GE varnish. The same experimental setup was successfully applied to determine the magnetic structure of the similar $EuPdSn_2$ compound [12].

Structural refinements were carried out according to the Rietveld method [15] using the program FULLPROF [16]. For XRPD data, a file describing the instrumental resolution function (obtained by analyzing a standard LaB_6 sample) and a Thompson-Cox-Hastings pseudo-Voigt convoluted with an axial divergence asymmetry function were used in the calculations. In the final cycle, the following parameters were refined: the scale factor, the zero point of the detector, the background, the unit cell parameters, the atomic site coordinates not constrained by symmetry, the atomic displacement parameters, and the anisotropic microstrain broadening using the parameters described in [17] tracing back to an approach presented in [18]. For the NPD data, Rietveld refinement was carried out by fitting the difference pattern obtained by subtracting the pattern collected at 20 K in the paramagnetic state, from data collected at 2.5, 5, 7.5, and 10 K (where magnetic ordering occurs). The resulting difference patterns consist of purely magnetic Bragg peaks.

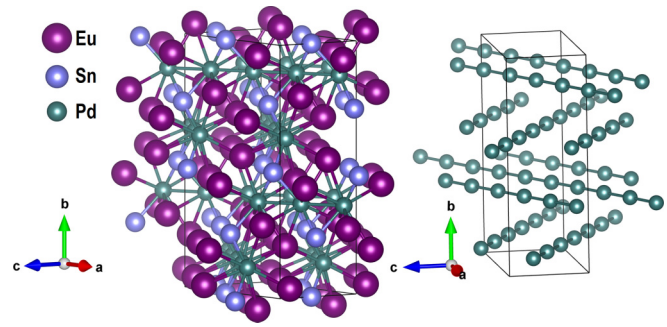

FIG. 1. Representation of the crystal structure of Eu_2Pd_2Sn; the drawing on the right shows the arrangement of the linear Pd chains.

III. RESULTS AND DISCUSSION

A. Structural description

So far, Eu_2Pd_2Sn is the only rare-earth representative crystallizing in the noncentrosymmetric orthorhombic structure with an $Fdd2$ symmetry (space group type no. 43; Fig. 1) [19]. It is isotypic with Ca_2Pd_2Ge [20], Sr_2Pd_2Al [21], and Sr_2Pd_2Sn [22].

In this crystal structure, the coordination polyhedra do not have a simple shape and there is no preferred polyhedron around a particular atom. The most remarkable structural feature is the linear chains connecting equidistant Pd atoms (spaced by ∼3 Å) lying in the *ac* plane (Fig. 1, on the right). These linear Pd chains are stacked along the *b*-axis and rotated by about 58.5°. A similar structural feature characterizes $CoIn_2$, where equidistant Co-Co chains are present; this compound crystallizes in the minimal nonisomorphic supergroup $Fddd$ symmetry at room temperature, but undergoes a structural transition driven by a Peierls distortion at low temperature where the atomic chains are distorted leading to the formation of Co pairs [23]. It is thus evident that a detailed investigation of the structural properties of Eu_2Pd_2Sn at low temperatures is required to ascertain if the Peierls distortion takes place also in Pd chains.

B. Synchrotron x-ray powder diffraction

Rietveld refinements carried out using synchrotron XRPD data reveal that Eu_2Pd_2Sn crystallizes in the $Fdd2$ space group type in the thermal range 4–290 K; no evidence of a structural transition (selective peak splitting or broadening) was detected. In particular, no incommensurate peaks were detected at low temperature, suggesting that the Peierls instability observed in $CoIn_2$ [23] is not active in Eu_2Pd_2Sn. Small amounts of Eu_2Pd_3Sn (∼8 wt. %) and other

TABLE I. Structural data of Eu_2Pd_2Sn at 290 K (upper data) and 4 K (lower data) obtained by Rietveld refinement (synchrotron XRPD data); space group type $Fdd2$ (space group no. 43).

Lattice parameters (Å)				
A		*B*		*c*
10.4825(1)		16.0739(1)		5.8739(1)
10.4057(1)		16.0343(1)		5.8556(1)
Atomic positions				
Atom	Wyckoff site	*x*	*y*	*z*
Eu	16*b*	0.1693(1)	0.0486(1)	0.083(7)
		0.1693(1)	0.0483(1)	0.082(9)
Pd	16*b*	0.6671(1)	0.1248(1)	0.075(7)
		0.6681(1)	0.1249(1)	0.075(9)
Sn	8*a*	½	0	0.089(7)
				0.092(9)
Agreement factors				
$R_{F-factor}$	3.66		R_{Bragg}	6.88
	2.49			6.04

unidentified secondary phase(s) were detected. The structural data for Eu_2Pd_2Sn at 4 and 290 K are listed in Table I, whereas Fig. 2 shows the Rietveld refinement plot obtained using the XRPD data collected at 4 K. The inset in Fig. 2 depicts the tensor surfaces representing the direction dependence of the microstrain broadening at 4 and 290 K; no significant change is observed at these temperatures, indicating that no change in crystal symmetry (even very subtle) occurs.

The thermal expansion behavior of Eu_2Pd_2Sn was investigated by fitting the cell volume in the thermal range 4–290 K (Fig. 3), using a second-order Grüneisen approximation for the equation of state at zero-pressure [24]:

$$V(T) = \frac{V_0 U}{Q - bU} + V_0, \tag{1}$$

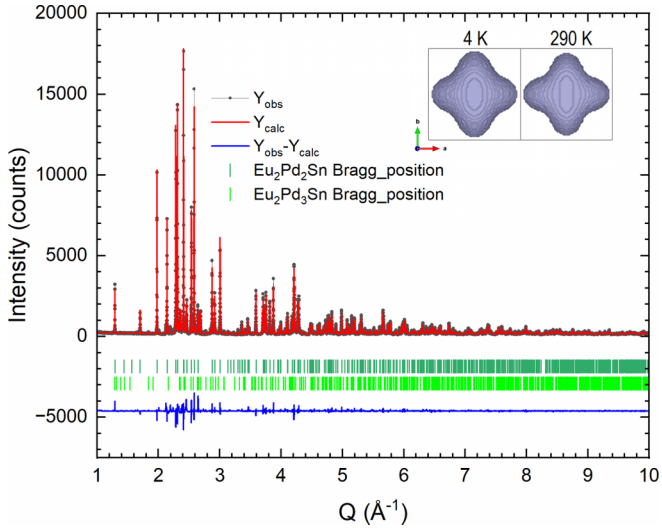

FIG. 2. Rietveld refinement plot for Eu_2Pd_2Sn (synchrotron XRPD data collected at 4 K); the inset shows the tensor surfaces representing the direction dependence of the microstrain broadening at 4 and 290 K.

where $Q = V_0K_0/\gamma'$ and $b = (K_0' - 1)/2$; γ' is a dimensionless Grüneisen parameter of the order of unity; K_0 is the compressibility, and K_0' is its derivative with respect to applied pressure; V_0 is the zero-temperature limit of the unit cell volume; and U is the internal energy per unit cell calculated by the Debye approximation:

$$U(T) = 9Nk_BT\left(\frac{T}{\Theta_D}\right)^3 \int_0^{\frac{T}{\Theta_D}} \frac{x^3 dx}{e^x - 1}, \tag{2}$$

where N is the number of atoms in the unit cell, k_B is the Boltzmann constant, Θ_D is the Debye temperature, and T is the temperature. The fit was carried out assuming $K_0 \sim$ 119.84 GPa as obtained by using high-pressure synchrotron XRPD data collected in a previous experiment on the similar compound Yb_2Pd_2In [25] (K_0 was calculated as described in Ref. [26]) and $\Theta_D = 177$ K obtained for Eu_2Pd_2Sn by

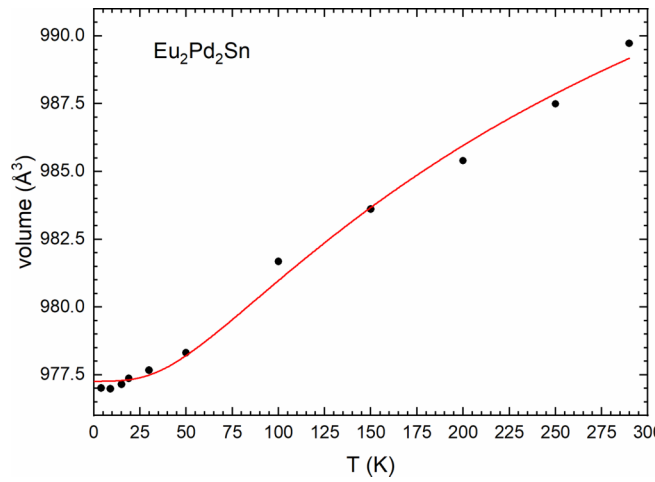

FIG. 3. Thermal evolution of the cell volume; the solid line represents the best fit to a second-order Grüneisen approximation.

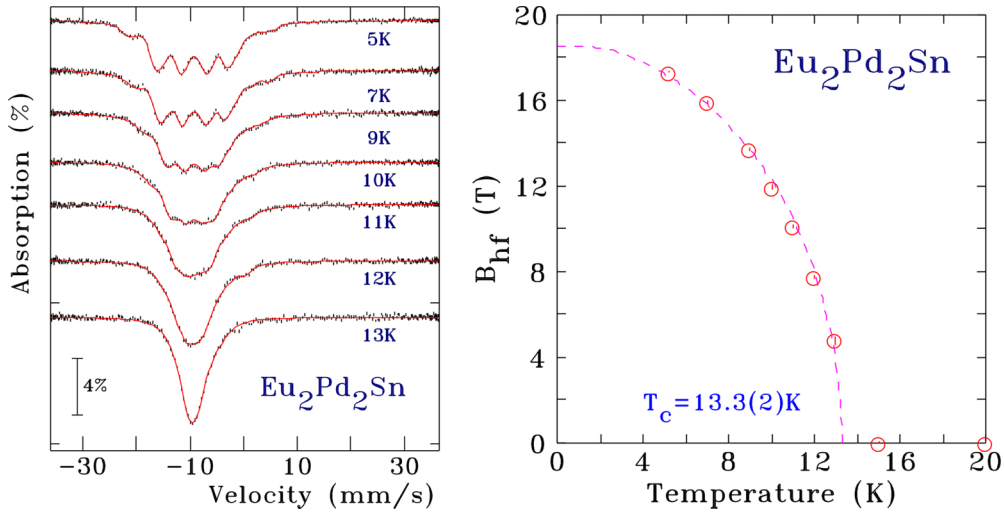

FIG. 4. Left: ^{151}Eu Mössbauer spectra of Eu_2Pd_2Sn at several temperatures; the solid lines are full Hamiltonian fits. Right: Temperature dependence of B_{hf} for Eu_2Pd_2Sn; the dashed line through the data is a mean-field solution to the Brillouin function fitting (with a $J = 7/2$ for Eu^{2+}) yielding an ordering temperature of ∼13.3 K.

low specific heat measurements [9]; γ' and K_0' were free parameters.

The Grüneisen approximation accounts reasonably well for the observed temperature evolution of the cell volume; a slight deviation is observed below ∼15 K, caused by magnetostriction in the magnetic phase.

C. ^{151}Eu Mössbauer spectroscopy

The ^{151}Eu Mössbauer spectrum of Eu_2Pd_2Sn at room temperature was recently reported to consist of a single line with an isomer shift of −9.48(1) mm/s [22], indicating that the europium is fully divalent. Our measurements were carried out in the paramagnetic regime at 15 K; the ^{151}Eu spectrum still consists of a single signal with an isomer shift of −9.08(2) mm/s confirming a divalent state for Eu; no evidence for Eu^{3+} can be detected (the detection limit for Eu^{3+} is ∼1%).

Fitting the spectrum taken at 5 K yields an isomer shift of −9.13(2) mm/s and a quadrupole interaction of −12.4(1) mm/s, with an average hyperfine field B_{hf} of 17.1(1) T, typical of divalent europium intermetallic compounds. Figure 4, on the left, shows the ^{151}Eu Mössbauer spectra of Eu_2Pd_2Sn at selected temperatures, clearly showing the evolution from magnetically split at 5 K to paramagnetic around 13 K (the solid lines are full Hamiltonian fits). A single Eu site fails to properly fit the spectrum collected at 5 K. Following the indication given by the NPD analysis (which reveals a distribution of moment orientations within the crystallographic cell due to cycloidal ordering; *vide infra* Sec. III C), the spectrum at 5 K was modeled using first two and then three equal-area subspectra with the isomer shifts and V_{zz} constrained to be equal (rotations cannot affect them) and both $|B_{hf}|$ and the angle between V_{zz} and B_{hf} as free parameters. This three-site model was found to work better than the two-site model at 5 K. The independent hyperfine fields and angles provide a simple way to model the distribution resulting from the cycloidal order. We found a small spread in the hyperfine field (+/–0.5 T) and in the angle (+/–30 deg). For $T > 5$ K, the differences between the two-site and three-site models rapidly became less significant, so in the interests of minimizing the free parameters used to fit the spectra, the two-site model was adopted above 5 K. While this approach is definitely an imperfect way to deal with the distribution of moment directions that characterizes the cycloidal ordering, it captures the essential form of the spectra with the minimum of additional parameters. Finally, the very narrow range of hyperfine fields seen in these spectra also indicates that no modulation of moments is involved in the magnetic order and thus all magnetic moments are essentially equivalent.

The hyperfine field shows a smooth evolution with temperature, which can be fitted with a mean-field solution of the Brillouin function with $J = 7/2$ for Eu^{2+} (Fig. 4, on the right), giving a transition temperature of 13.3(2) K.

D. Neutron powder diffraction

Upon cooling, magnetic Bragg peaks arise in the NPD patterns below ∼14 K (Fig. 5). The magnetic diffraction pattern is dominated by a low-angle peak at 0.25 $Å^{-1}$ that cannot be indexed to the crystallographic cell; several other weak incommensurate magnetic satellite reflections are clearly observed at higher Q values, which strongly change their positions with temperature.

The position of the $000^{\pm}$ peak at 0.25 $Å^{-1}$ exhibits a peculiar behavior (Fig. 6). In fact, on cooling, it initially shifts to lower Q values just below the magnetic transition, it reaches a minimum, and then as the temperature is further lowered, it shifts again to higher Q values.

To determine the possible magnetic structures compatible with the symmetry of the underlying nuclear structure, the magnetic propagation wave vector **k** was identified using the program K-search; representation analysis was then carried using the program BASIREPS [27]; both software are included in the FULLPROF suite of programs. As a result, the magnetic peak positions fit with a $\mathbf{k} = [\delta_x, \delta_y, 0]$ type magnetic wave

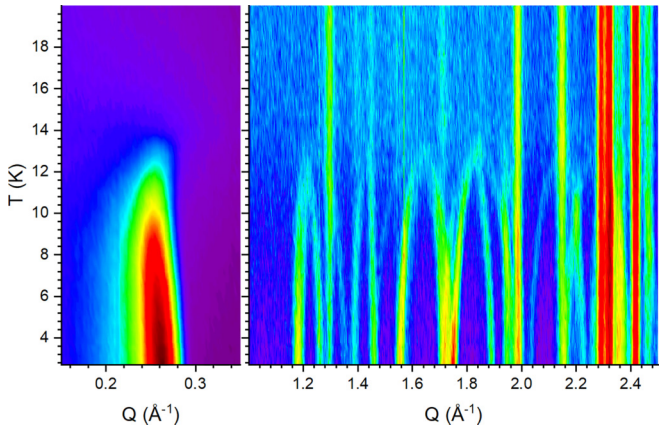

FIG. 5. Temperature-dependent evolution of the magnetic Bragg peaks in Eu_2Pd_2Sn (NPD data; panels have different colors scales; red: high intensity, violet: low intensity).

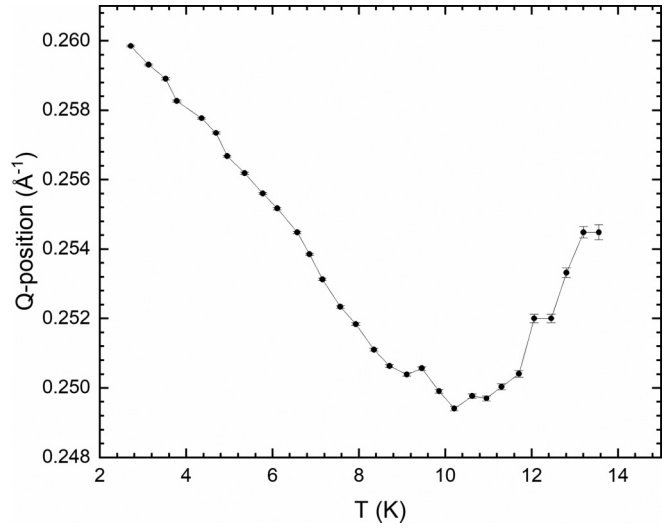

FIG. 6. Temperature dependence of the $000^{\pm}$ magnetic peak position (NPD fast scan data).

vector; the very strong magnetic peak at low $Q = 0.25\,\text{Å}^{-1}$ actually corresponds to the $000^{\pm}$ magnetic peak. For this magnetic propagation vector, symmetry analysis returns a single magnetic irreducible representation with independent Fourier coefficients along the main axes for Eu at the 16*b* site.

Due to the strong neutron absorption of Eu (which reduces the intensity of the coherent scattering), the Rietveld refinements of the magnetic structure were carried out by fitting the difference pattern obtained by subtracting the data collected in the paramagnetic regime at 20 K from those collected at 2.5 K (Fig. 7, on the left) to obtain a difference plot that consists of purely magnetic Bragg peaks. The value of the scale-factor (needed to calculate the absolute values of the magnetic moments) was obtained by refinements using the data collected at 20 K, where only nuclear Bragg peaks are present. A good refinement of this difference data set was obtained assuming a magnetic structure characterized by an incommensurate cycloidal ordering of the Eu magnetic moments in the *ac* plane. The components of the magnetic moment were identical within the error bars along the *a*- and *c*-directions and were therefore constrained to the same value. This is consistent with the Mössbauer data, which suggest that all magnetic moments should be equivalent. There is no component along the *b*-axis. The final refinement of the 2.5–20 K difference data shown in Fig. 7, on the left, with $R_{\text{magn}} = 13.1\%$ was obtained using just three free parameters: the magnetic moment value, $\mu_{\text{Eu}} = 5.97(2)\mu_{\text{B}}$, and the two components of the magnetic propagation wave vector $\mathbf{k} = [0.3557(6),\ 0.326(1),\ 0]$. The observed cycloidal magnetic structure has no center of inversion symmetry, like the underlying nuclear structure.

In a magnetic transition, the order parameter η corresponds to the ordered magnetic moment value, which is linearly proportional to the squared value of the intensity of the magnetic Bragg peak intensity. For this purpose, the integrated intensity of the very strong magnetic Bragg peak $000^{\pm}$ centered at $0.25\,\text{Å}^{-1}$ (arising at $T < 13.96$ K) was determined from the temperature-dependent data. Figure 8 (on the left) shows the square root intensity data fitted with a mean-field solution of the Brillouin function with $J = 7/2$ for Eu^{2+} (as for ^{151}Eu Mössbauer data), yielding $T_m \sim 14.1$ K. In comparison with the ^{151}Eu Mössbauer data fitting (Fig. 4) (as well as susceptibility measurements and specific-heat measurements [19]), the magnetic transition temperature is slightly increased because the NPD data were collected in a continuous mode during heating.

The components of the magnetic propagation vector obtained by Rietveld refinements using fast-scan NPD data are displayed as a function of temperature in Fig. 8 on the right. Both components change with temperature, but they never assume a commensurate value. Just below the magnetic transition, the component along the *y*-axis exhibits a notable change, whereas the component along the *x*-axis decreases slightly upon cooling. In particular, the $\mathbf{k}_x$ component tends to lock below ~5.5 K, whereas the $\mathbf{k}_y$ component still evolves down to 2.5 K. The minimum observed in the temperature dependence of the $000^{\pm}$ magnetic peak position (Fig. 6) thus originates from the evolution of the two components of the magnetic propagation wave vector.

The magnetic structure of Eu_2Pd_2Sn is somehow similar to that of $EuNiGe_3$ [28], which also crystallizes in a non-centrosymmetric structure (space group type: $I4mm$). Indeed, an incommensurate helicoidal ordering develops in $EuNiGe_3$ along both the *a*- and *b*-axes in the Eu substructure, and the magnetic moment exhibits non-null components along all three main basis vectors.

IV. CONCLUSIONS

The crystal structure of Eu_2Pd_2Sn was investigated in the thermal range of 4–290 K using synchrotron x-ray powder diffraction; no structural transition takes place in this temperature range. ^{151}Eu Mössbauer spectroscopy and neutron powder diffraction show the occurrence of a second-order magnetic transition at $T_m \sim 13.8(5)$ K. In particular, Eu_2Pd_2Sn adopts a complex magnetic structure, characterized by an incommensurate cycloidal ordering of Eu magnetic moments with a magnitude of $5.97(2)\mu_{\text{B}}$ and a magnetic propagation wave vector $\mathbf{k} = [0.3557(6), 0.326(1), 0]$ at 2.5 K.

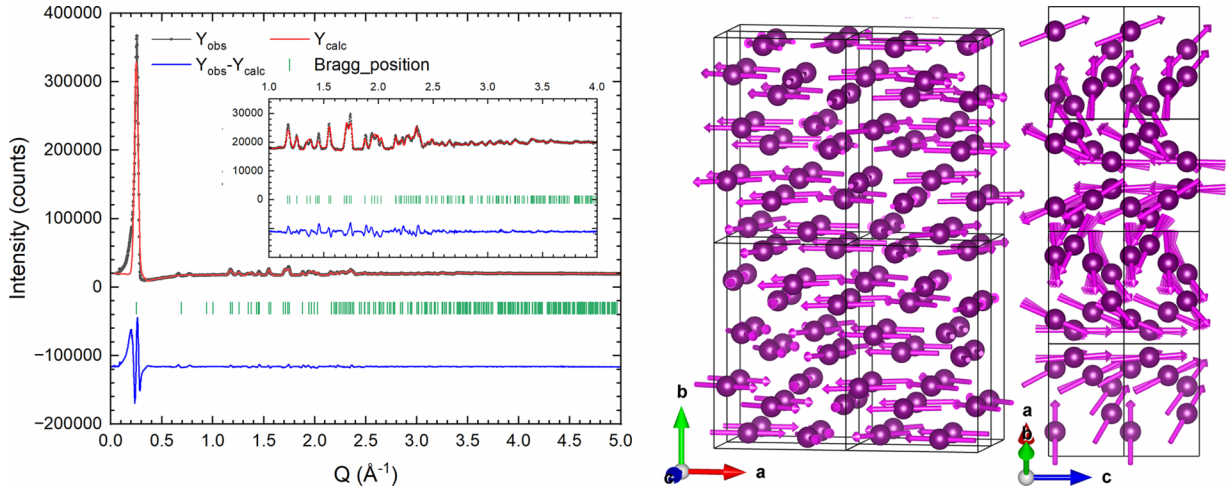

FIG. 7. Left: Difference plot fitting of the NPD magnetic Bragg peaks of Eu_2Pd_2Sn at 2.5 K; the inset is a magnification of the plot in the $1-4\,\text{Å}^{-1}$ Q-range. Right: Representation of the Eu incommensurate cycloidal magnetic moments orderings along two different crystallographic directions.

Eu_2Pd_2Sn exhibits significant structural and magnetic analogies to $EuNiGe_3$, possibly indicating the formation of a skyrmion lattice state also in this compound.

ACKNOWLEDGMENTS

This work was carried out with the support of the European Synchrotron Radiation Facility (proposal HC-4363; DOI:10.15151/ESRF-ES-447344408) and Institute Laue-Langevin (proposal DIR-231; DOI: 10.5291/ILL-DATA.DIR-231). A.M. acknowledges A. Fitch for his kind assistance during data collection at ID22. Financial support for this work was provided by Fonds Québécois de la Recherche sur la Nature et les Technologies, and the Natural Sciences and Engineering Research Council (NSERC) Canada.

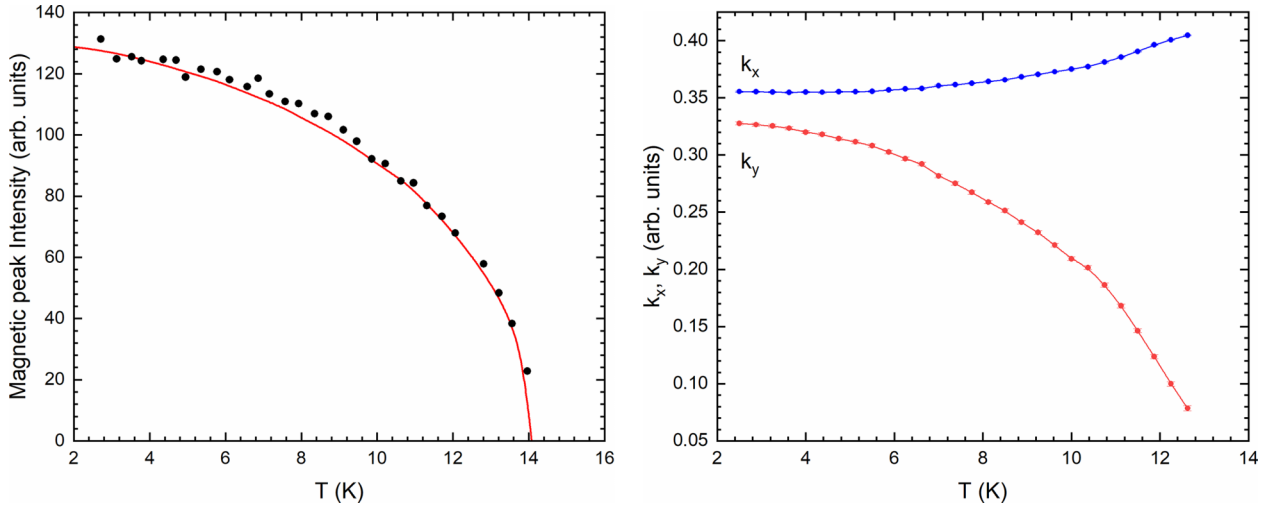

FIG. 8. NPD fast scan data. Left: thermal dependence of the square root intensity of the magnetic Bragg peak $000^{\pm}$; the continuous line represents the fit with a mean-field solution of the Brillouin function with $J = 7/2$ for Eu^{2+}. Right: Components of the magnetic propagation vector plotted as a function of temperature (lines are a guide to the eye).

[1] Y. Togawa, T. Koyama, K. Takayanagi, S. Mori, Y. Kousaka, J. Akimitsu, S. Nishihara, K. Inoue, A. S. Ovchinnikov, and J. Kishine, Chiral magnetic soliton lattice on a chiral helimagnet, Phys. Rev. Lett. **108**, 107202 (2012).

[2] N. Nagaosa and Y. Tokura, Topological properties and dynamics of magnetic skyrmions, Nat. Nanotechnol. **8**, 899 (2013).

[3] A. Fert, M. Chshiev, A. Thiaville, and H. Yang, From early theories of Dzyaloshinskii–Moriya interactions in metallic systems to today's novel roads, J. Phys. Soc. Jpn. **92**, 081001 (2003).

[4] S. Mühlbauer, B. Binz, F. Jonietz, C. Pfleiderer, A. Rosch, A. Neubauer, R. Georgii, and P. Böni, Skyrmion lattice in a chiral magnet, Science **323**, 915 (2009).

[5] A. Bauer, A. Senyshyn, R. Bozhanova, W. Simeth, C. Franz, S. Gottlieb-Schönmeyer, M. Meven, T. E. Schrader, and C. Pfleiderer, Magnetic properties of the noncentrosymmetric tetragonal antiferromagnet $EuPtSi_3$, Phys. Rev. Mater. **6**, 034406 (2022).

[6] J. A. M. Paddison, B. K. Rai, A. F. May, S. Calder, M. B. Stone, M. D. Frontzek, and A. D. Christianson, Magnetic interactions of the centrosymmetric skyrmion material Gd_2PdSi_3, Phys. Rev. Lett. **129**, 137202 (2022).

[7] S. V. Grigoriev, D. Chernyshov, V. A. Dyadkin, V. Dmitriev, E. V. Moskvin, D. Lamago, T. Wolf, D. Menzel, J. Schoenes, S. V. Maleyev, and H. Eckerlebe, Interplay between crystalline chirality and magnetic structure in $Mn_{1-x}Fe_xSi$, Phys. Rev. B **81**, 012408 (2010).

[8] W. Iha, S. Matsuda, M. Kakihana, A. Nakamura D. Aoki, M. Nakashima, Y. Amako, T. Takeuchi, M. Kimata, Y. Otani, M. Hedo, T. Nakama, and Y. Onuki, Anomalous Hall effect in antiferromagnet $EuNiGe_3$ with the Rashba-type tetragonal structure, JPS Conf. Proc. **30**, 011092 (2020).

[9] J. G. Sereni, I. Čurlík, M. Reiffers, and M. Giovannini, Evidence for magnetic dimers and skyrmion lattice formation in Eu_2Pd_2Sn, Phys. Rev. B **108**, 014427 (2023).

[10] M. Potter, H. Fritzsche, D. H. Ryan, and L. M. D. Cranswick, Low-background single-crystal silicon sample holders for neutron powder diffraction, J. Appl. Cryst. **40**, 489 (2007).

[11] P. Lemoine, J. M. Cadogan, D. H. Ryan, and M. Giovannini, The magnetic structure of EuPdSn, J. Phys.: Condens. Matter **24**, 236004 (2012).

[12] A. Martinelli, D. Ryan, J. Sereni, C. Ritter, A. Leineweber, I. Čurlík, R. Freccero, and M. Giovannini, Magnetic phase separation in the $EuPdSn_2$ ground state, J. Mater. Chem. C **11**, 7641 (2023).

[13] I. Čurlík, M. Giovannini, F. Gastaldo, A. M. Strydom, M. Reiffers, and J. G. Sereni, Crystal structure and physical properties of the two stannides $EuPdSn_2$ and $YbPdSn_2$, J. Phys. Condens. Matter **30**, 495802 (2018).

[14] C. J. Voyer and D. H. Ryan, A complete solution to the Mössbauer problem, all in one place, Hyperfine Interact. **170**, 91 (2006).

[15] R. A. Young, in *The Rietveld Method*, edited by R. A. Young, IUCr Monographs on Crystallography (Oxford University Press, Oxford, 1993), Vol. 5, pp. 1–38.

[16] J. Rodríguez-Carvajal, Recent advances in magnetic structure determination by neutron powder diffraction, Phys. B **192**, 55 (1993).

[17] J. Rodriguez-Carvajal and T. Roisnel, Line broadening analysis using fullprof: Determination of microstructural properties, Mater. Sci. Forum **443**, 123 (2004).

[18] J. Rodriguez-Carvajal, M. T. Fernandez-Diaz, and J. L. Martinez, Neutron diffraction study on structural and magnetic properties of La_2NiO_4, J. Phys. Condens. Matter **3**, 3215 (1991).

[19] M. Giovannini, I. Čurlík, R. Freccero, P. Solokha, M. Reiffers, and J. Sereni, Crystal structure and magnetism of noncentrosymmetric Eu_2Pd_2Sn, Inorg. Chem. **60**, 8085 (2021).

[20] I. Doverbratt, S. Ponou, Y. Zhang, S. Lidin, and G. J. Miller, Linear metal chains in Ca_2M_2X (M = Pd, Pt; X = Al, Ge): Origin of the pairwise distortion and its role in the structure stability, Chem. Mater. **27**, 304 (2015).

[21] F. Stegemann, C. Benndorf, R. St. Touzani, B. P. T. Fokwa, and O. Janka, Experimental and theoretical investigations of the polar intermetallics $SrPt_3Al_2$ and Sr_2Pd_2Al, J. Solid State Chem. **242**, 143 (2016).

[22] J. Wiethölter, A. Koldemir, M. Kai Reimann, T. Block, J. Kösters, O. Janka, and R. Pöttgen, Mössbauer-spectroscopic characterization of the stannides Sr_2Pd_2Sn and Eu_2Pd_2Sn, Z. Naturforsch. **78**, 301 (2023).

[23] N. L. Gulay, J. Kösters, Y. M. Kalychak, S. F. Matar, A. Rabenbauer, T. Nilges, and R. Pöttgen, Peierls distortion of the cobalt chain in the low-temperature structure of $CoIn_2$, Z. Kristallogr. **237**, 239 (2022).

[24] L. Vočadlo, K. S. Knight, G. D. Price, and I. G. Wood, Thermal expansion and crystal structure of FeSi between 4 and 1173 K determined by time-of-flight neutron powder diffraction, Phys. Chem. Miner. **29**, 132 (2002).

[25] G. Lamura, I. J. Onuorah, P. Bonfà, S. Sanna, Z. Shermadini, R. Khasanov, J.-C. Orain, C. Baines, F. Gastaldo, M. Giovannini, I. Curlík, A. Dzubinska, G. Pristas, M. Reiffers, A. Martinelli, C. Ritter, B. Joseph, E. Bauer, R. De Renzi, and T. Shiroka, Pressure-induced antiferromagnetic dome in the heavy-fermion $Yb_2Pd_2In_{1-x}Sn_x$ system, Phys. Rev. B **101**, 054410 (2020).

[26] A. Martinelli, M. Ferretti, A. Palenzona, and M. Merlini, The bulk modulus of $SmFeAs(O_{0.93}F_{0.07})$, Physica C **469**, 782 (2009).

[27] C. Ritter, Neutrons not entitled to retire at the age of 60: More than ever needed to reveal magnetic structures, Solid State Phenom. **170**, 263 (2011).

[28] D. H. Ryan, J. M. Cadogan, R. Rejali, and C. D. Boyer, Complex incommensurate helicoidal magnetic ordering of $EuNiGe_3$, J. Phys.: Condens. Matter **28**, 266001 (2016).